nature photonics

LETTERS

PUBLISHED ONLINE: 26 JUNE 2011 | DOI: 10.1038/NPHOTON.2011.125

Lensless imaging using broadband X-ray sources

Brian Abbey[1], Lachlan W. Whitehead[1], Harry M. Quiney[1], David J. Vine[1], Guido A. Cadenazzi[1], Clare A. Henderson[1], Keith A. Nugent[1]*, Eugeniu Balaur[2], Corey T. Putkunz[2], Andrew G. Peele[2], G. J. Williams[3] and I. McNulty[4]

High-resolution X-ray imaging techniques using optical elements such as zone plates are widely used for viewing the internal structure of samples in exquisite detail. The resolution attainable is ultimately limited by the manufacturing tolerances for the optics. Combining ideas from crystallography and holography, this limit may be surpassed by the method of coherent diffractive imaging (CDI)[1]. Although CDI shows particular promise in applications involving X-ray free-electron lasers[2], it is also emerging as an important new technique for imaging at third-generation synchrotrons. The limited coherent output of these sources, however, is a significant barrier to obtaining shorter exposure times. A fundamental assumption of coherent diffractive imaging is that the incident light is well-approximated by a single optical frequency. In this Letter, we demonstrate the first experimental realization of 'polyCDI', using a broadband source to achieve a factor of 60 reduction in the exposure time over quasi-monochromatic coherent diffractive imaging.

Over the past decade, the extension of crystallographic techniques to the high-resolution imaging of non-crystalline objects[3] has proved enormously successful in a wide variety of applications[4]. Iterative retrieval of the phase of the far-field diffraction pattern permits reconstruction of the diffracting object with a spatial resolution that is limited, in principle, only by the wavelength of the incident illumination. In crystallography, the periodic arrangement of atoms amplifies the signal diffracted from the unit cell, making detection of the Bragg peaks straightforward. A main goal for coherent diffractive imaging (CDI) is to develop it into a form of high-spatial-resolution microscopy that can be routinely applied using synchrotron sources. In this endeavour it must compete with the very successful results obtained using zone-plate-based full-field transmission X-ray microscopy[5]. A fundamental issue for both forms of imaging is that higher spatial resolution requires that the sample be illuminated with a greater number of photons per resolution element, scaling approximately as the fourth power of the desired spatial resolution[6]. Although it has been asserted that CDI is able to achieve equivalent resolution to zone plate microscopy, but with fewer photons[7], the two techniques are limited to precisely the same degree by the spectral bandwidth (longitudinal coherence length) of the incident light. Significant increases in the spatial resolution require brighter sources, much longer exposure times or the capacity to increase the acceptable limits on the bandwidth. A pathway to achromatic zone plates has been proposed[8] that claims a potential for two orders of magnitude improvement in the allowed bandwidth. In the present Letter we experimentally demonstrate a comparable improvement in the acceptable spectral bandwidth for CDI.

CDI generally assumes full temporal and spatial coherence, and even relatively small deviations from full coherence can prevent the algorithm from converging correctly[9,10]. In spite of the recent success of CDI, the assumption of full coherence is only an approximation to the experimental situation. Recent developments in the field of table-top X-ray sources, for example, would benefit significantly from techniques that use the full bandwidth of the source[11]. In addition, many non-resonant structural problems, particularly biological applications where the dose-optimal energies are well above the edges of low-Z elements, could take advantage of broadband light. The approach could also be used to take advantage of the full bandwidth of a self-amplified spontaneous emission (SASE) pulse ($E/\mathrm{d}E \approx 1{,}000$) from an X-ray free-electron laser (XFEL) in cases where the path-length difference would otherwise be prohibitive for CDI. An important example would be the imaging of large molecules at high resolution. For sources with partial spatial coherence, the effects can be accommodated provided the coherence properties are well-characterized[10]. Here, we address another underlying coherence assumption of CDI, namely that the far-field diffraction data must be formed using a quasi-monochromatic incident wave-field. Our results show that an X-ray source comprising a relatively broad continuous frequency distribution can be used for diffractive imaging provided a priori knowledge of the power spectrum is included in the reconstruction. The approach yields a 60-fold reduction in exposure time.

The far-field propagated wave can be described by the Fourier transform of the fully coherent exit surface wave. When the illumination contains a continuous frequency distribution, the contribution from all wavelengths within the spectrum must be considered (Step 5 of the polyCDI algorithm in the Methods). Provided the observation time is much longer than the coherence time of the incident wave-field, the polychromatic far-field diffraction pattern can be described as a spectrally weighted incoherent sum over the intensity distribution produced by each incident wavelength. This is, in a sense, a generalization of the modal formulation of the cross-spectral density given in ref. 12. This representation assumes that the distribution does not span any absorption edges, that it is sufficiently narrow that dispersive effects within the sample can be ignored, and that the scattering angle is small. Within these assumptions, the different wavelengths simply act to rescale the diffraction pattern (Step 6 of the PolyCDI algorithm in the Methods). Multiple-wavelength diffractive imaging using a high-harmonic generation (HHG) X-ray source has previously been demonstrated[13]. In that case, however, only six modes corresponding to the six well-separated narrow harmonics (each represented by a single optical frequency) were propagated to the detector plane to retrieve the phase of the diffraction pattern.

[1]ARC Centre of Excellence for Coherent X-ray Science, School of Physics, The University of Melbourne, Victoria 3010, Australia, [2]ARC Centre of Excellence for Coherent X-ray Science, Department of Physics, La Trobe University, Bundoora, Victoria 3086, Australia, [3]SLAC National Accelerator Laboratory, 2575 Sand Hill Road, Menlo Park, California 94025, USA, [4]Advanced Photon Source, Argonne National Laboratory, Argonne, Illinois 60439, USA.
*e-mail: keithan@unimelb.edu.au

© 2011 Macmillan Publishers Limited. All rights reserved.

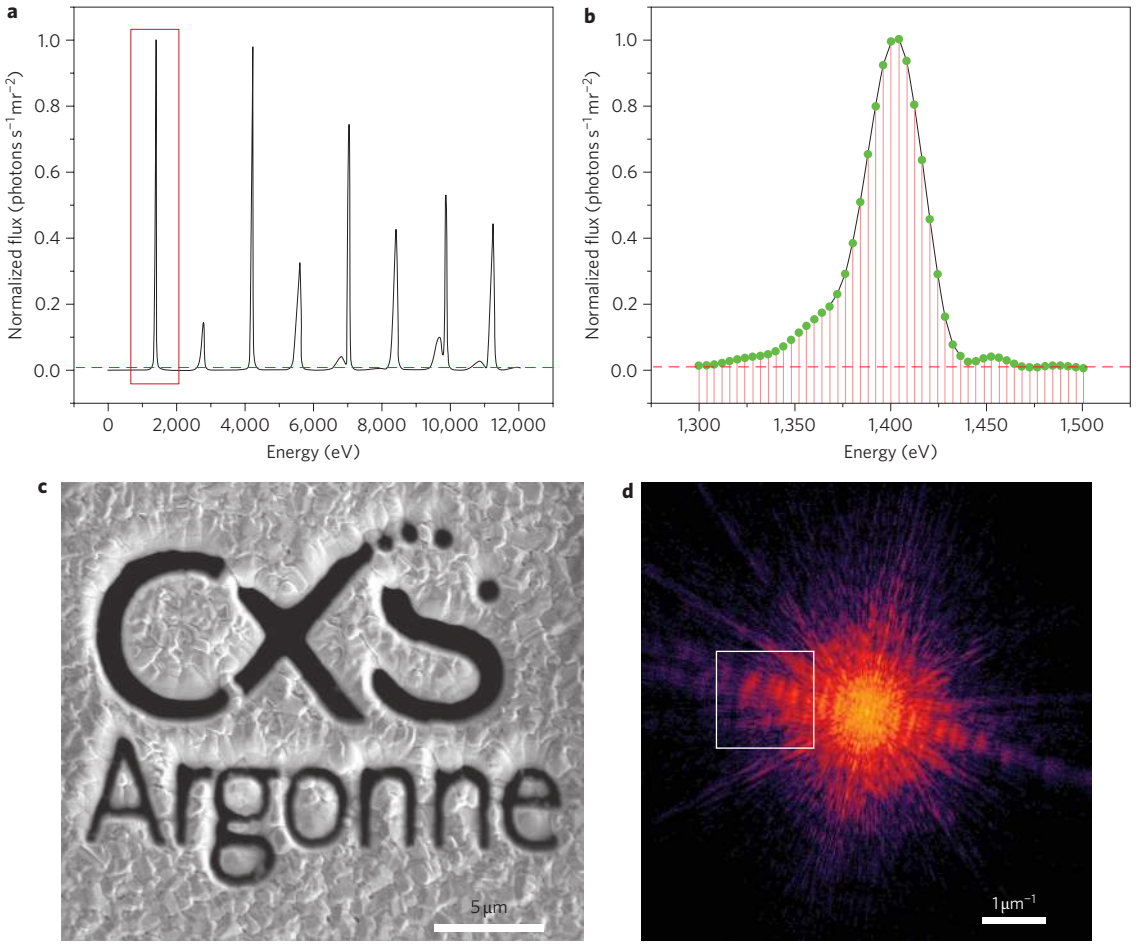

Figure 1 | Polychromatic data and sample. a, Undulator spectrum for beamline 2-ID-B at the APS generated using SPECTRA software. **b**, First harmonic with peak energy at ~1.4 keV. Green circles indicate the 51 points at which the spectrum was sampled for input into the polychromatic CDI reconstruction code. **c**, SEM image of the test object ($D = 15$ μm), which was prepared using focused ion beam machining from a 1-μm-thick gold film. **d**, Measured intensity (logarithmically scaled) at the detector using the illumination characterized in **b**.

The 512 samples mentioned in ref. 13 were only used to reconstruct the spectrum and not for the phase retrieval. This situation is quite different to the present case, where a finely sampled, broadband continuous spectrum is used. The method described here is a much more general approach, and could also be used for phase retrieval based on a discrete spectrum. The multiple-wavelength method[13] could not, however, be used to analyse data produced by a continuous spectrum.

The experiment was carried out at the 2-ID-B undulator beamline at the APS[14] using a conventional plane-wave CDI setup. A 1.4 keV X-ray beam with a bandwidth of ~0.08% was selected with a 5.5 cm period (U5.5) undulator and spherical grating monochromator (SGM). The widths of the entrance and exit slits were 40 μm and 5 μm, respectively; the spatial and temporal coherence lengths at comparable slit settings and energy have been measured previously[10,15]. The diffraction data were collected using a peltier-cooled charge-coupled device (CCD) with 2,048 × 2,048 pixels, each 13.5 × 13.5 μm, placed 1.3 m downstream of the sample. For the polyCDI experiment, the zero order of the monochromator was used so that the full first undulator harmonic (peak energy, ~1.4 keV) was available.. The undulator spectrum was calculated using SPECTRA software[16], which relies on analytical expressions derived for undulator radiation in the near-field using the known parameters for 2-ID-B[17]. The bandwidth derived from the full-width at half-maximum (FWHM) of this spectrum (Fig. 1) is $\Delta\lambda/\lambda \approx 2.8\%$, which is comparable to the value of 2.3% obtained directly from the number of magnetic periods. The factor of 60 quoted for the improvement in exposure time is the ratio of the time to detector saturation, limited by the detector dynamic range, with a polychromatic beam compared to a quasi-monochromatic beam. This factor may be readily explained in terms of the ratio of the areas under the monochromator peak compared to the full undulator peak and the efficiency of the SGM (Supplementary Data S3). The minimum sampling frequency for the incident spectrum depends on the detector pixel size and the range of frequencies present in the spectrum (Supplementary Fig. S1). For the present geometry, a sampling frequency of 40 Å^{-1} of the spectrum was found to be sufficient to represent the polychromatic diffraction pattern.

According to Abbé[18], the highest obtainable resolution Γ in a fully coherent CDI reconstruction is given by $\Gamma = \lambda/2 \sin\theta$, where θ is the largest half-angle out to which the diffraction pattern can be reliably phased[4]. For a finite longitudinal coherence, the maximum path length over which interference may be observed will limit the resolution to a value given by

$$\Gamma = \frac{\bar{\lambda} D}{2 l_c} \qquad (1)$$

where D is the largest characteristic dimension of the object (15 μm in the current experiment), $\bar{\lambda}$ is the central wavelength of the

© 2011 Macmillan Publishers Limited. All rights reserved.

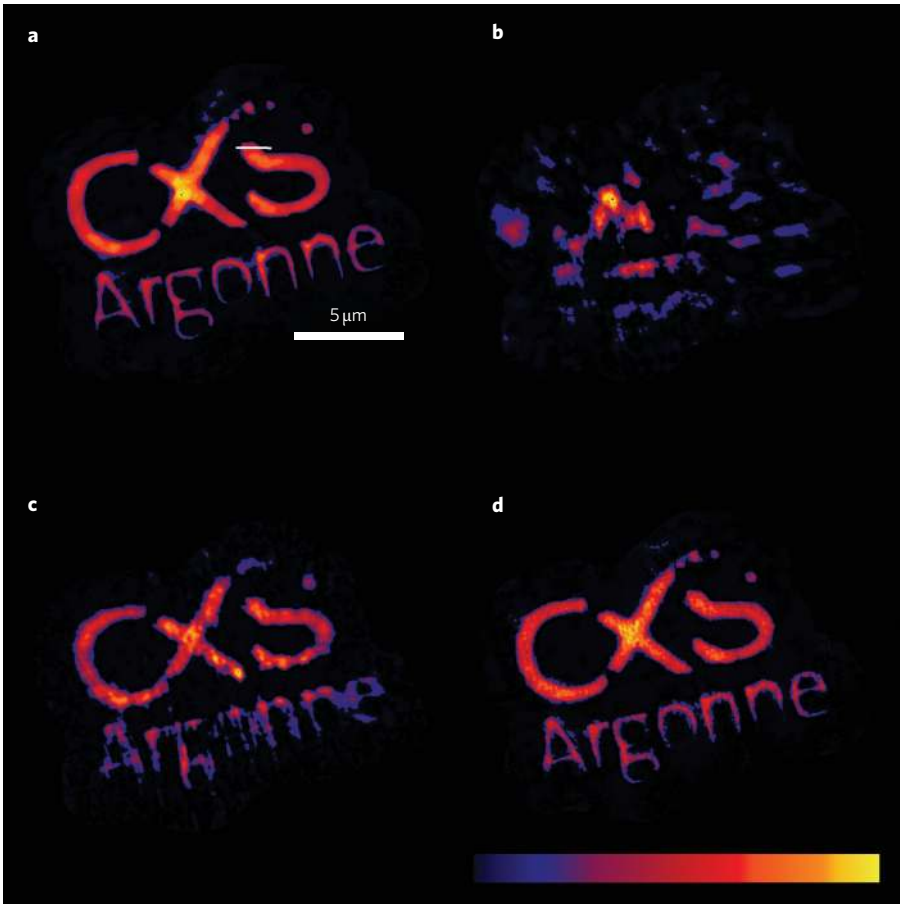

Figure 2 | Reconstructed amplitude of sample ESW from the test object shown in Fig. 1c multiplied by the final sample support (identical for each reconstruction). All reconstructions presented here use known spatial coherence information (multimodal propagation) for illumination. **a**, Reconstruction from quasi-monochromatic data, collected with 500 × 3 s exposures, assuming full temporal coherence. **b**, Reconstruction from polychromatic data, collected with 500 × 50 ms exposures, assuming full temporal coherence; that is, using an identical procedure to **a**, the data could not be reconstructed. **c**, Reconstruction from polychromatic data assuming full temporal coherence but using the exact dimensions of the object (obtained from **a**) as the initial support. **d**, Reconstruction from polychromatic data using an identical procedure to **a** and **b** but using the polychromatic diffraction algorithm.

incident light (see Methods) and l_c is the longitudinal coherence length. This expression assumes the paraxial approximation. In terms of the FWHM of the incident beam, the longitudinal coherence length is defined as $l_c = \bar{\lambda}^2/\Delta\lambda$. For the present experiment, equation (1) gives the maximum allowed bandwidth as $\Delta\lambda/\lambda = 1.4 \times 10^{-2}$. For a full undulator harmonic $\Delta\lambda/\lambda \approx 3.7 \times 10^{-2}$, suggesting that, without compensation, a substantial loss in resolution will result. The above estimates indicate that the FWHM of a full undulator harmonic is three times larger than the maximum value that can be tolerated using quasi-monochromatic CDI; in practice, we expect this factor to be considerably larger because equation (1) is probably an idealized limit not achievable in practice[19]. An analytical expression for the maximum allowed bandwidth using polyCDI is derived in Supplementary Data S2. The theoretical limit on the bandwidth using polyCDI for this experiment is 11%, eight times larger than the maximum theoretical bandwidth for quasi-monochromatic CDI. Note that although the spatial coherence length will likely change with wavelength, the bandwidth of the incident light is sufficiently small that the consequent change in spatial coherence length is within experimental errors for its measurement, and well within the tolerances required for the application of our treatment of the effect of spatial coherence[10].

The reconstructed sample exit surface wave (ESW) for quasi-monochromatic (total exposure time, 25 min) and polychromatic data (total exposure time, 25 s) is shown in Fig. 2. To make a direct comparison between the results, an identical reconstruction procedure was carried out for each (Supplementary Data S3). Iteration between the sample plane and detector plane was carried out using a combination of the hybrid input–output (HIO) and error reduction (ER) algorithms[20]. The three reconstructions based on the polychromatic data show varying levels of quality depending on the method used. Both CDI, using quasi-monochromatic data and polyCDI with the power spectrum explicitly included in the reconstruction algorithm, converged to a solution after 700–1,000 iterations.

Figure 3 shows the broadband diffraction data; the polychromatic data are clearly less sharp than the quasi-monochromatic data. The resolution lineouts in Fig. 3 show that quasi-monochromatic and polyCDI nonetheless give indistinguishable profiles; both yield an experimental resolution of 150 ± 5 nm consistent with the Abbé fully coherent diffraction limit of 117 nm.

However, when a single wavelength was used to propagate the ESW to the far-field for the broadband data the algorithm failed to converge. To try and drive the single-wavelength CDI algorithm to a recognizable solution, the ESW phase recovered from the quasi-monochromatic data was used as a starting guess for a reconstruction of the polychromatic data. Applying ER saw the initial high-quality reconstruction of the object rapidly degrade. As a final test, a support corresponding to the outline of the quasi-monochromatic reconstruction was used to constrain the ESW in the sample

© 2011 Macmillan Publishers Limited. All rights reserved.

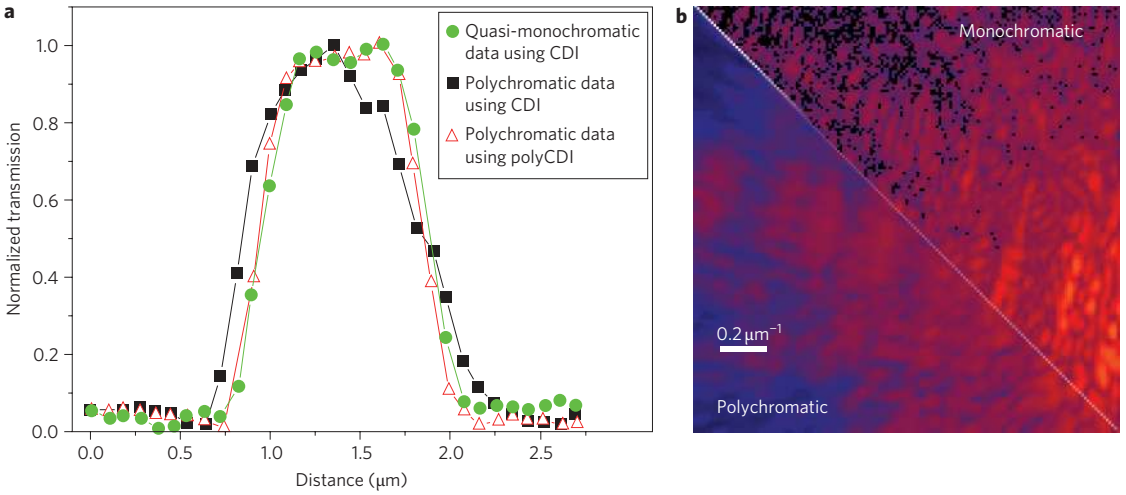

Figure 3 | Comparison of reconstructed image resolution and data. Example resolution lineout comparing the results from Fig. 2a, c and d. The data show that the reconstruction from quasi-monochromatic data (500 × 3 s exposures) gives a virtually identical profile to the polyCDI algorithm reconstruction (500 × 50 ms exposures). The experimentally determined resolutions measured from both sets of data are 150±5 nm. The result obtained from broadband data using just a priori knowledge of the sample to generate the support gives a significantly lower resolution of 320±7 nm. **b**, Comparison of the quasi-monochromatic and broadband data for the region bounded by the white box in Fig. 1d. The polychromatic diffraction pattern is significantly more blurred than the monochromatic equivalent, meaning that it cannot effectively be used to reconstruct the sample ESW without accounting for the spectral distribution.

plane and single-wavelength CDI then used to reconstruct the object. However, the quality of the image in this case was comparatively poor, though recognizable, and the spatial resolution (320± 7 nm) significantly reduced. After relaxing the support the reconstruction rapidly degraded until it was unrecognizable. We conclude that the broadband data would not be reconstructed using any algorithm that assumes quasi-monochromaticity. When the incident spectrum is sampled sufficiently finely, however, polyCDI recovers the sample ESW without loss of spatial resolution and, in our experiments, produced essentially identical image quality with an exposure time reduced by a factor of 60.

The ability to extend CDI to wide-bandwidth sources allows more than an order of magnitude reduction in the time taken to acquire the equivalent image using a quasi-monochromatic beam. This method will thus find immediate application in most forms of CDI and, in particular, has profound implications for coherent diffraction tomography for which large data sets are necessary[9].

Methods

The polyCDI algorithm used here fundamentally assumes that the cross-spectral density of an optical planar wave field $\psi_\lambda(\mathbf{r}_i, z_i)$ may be decomposed into a series of mutually incoherent modes[12]. The details of the modal propagation and phase retrieval of the polychromatic wave-field are given in the following.

The free-space propagation of $\psi_\lambda(\mathbf{r}_i, z_i)$ a distance $z_{ij} = z_j - z_i$ to $\psi_\lambda(\mathbf{r}_j, z_j)$ is given within the far-field approximation as

$$\psi_\lambda(\mathbf{r}_j, z_j) = -\frac{i}{\lambda z}\exp\left(\frac{2\pi i z_{ij}}{\lambda}\right)\exp\left(\frac{i\pi \mathbf{r}_j^2}{\lambda z_{ij}}\right)\iint \psi_\lambda(\mathbf{r}_i, z_i)\exp \times\left(-\frac{2\pi i \mathbf{r}_i\cdot\mathbf{r}_j}{\lambda z_{ij}}\right)\mathrm{d}\mathbf{r}_i \quad (2)$$

where λ is the wavelength and $\mathbf{r}_i$ and $\mathbf{r}_j$ define the position perpendicular to the beam in the sample planes z_i and detector planes z_j, respectively. In terms of the Fourier transform operator $\mathcal{F}$, equation (2) is defined as

$$\psi_\lambda(\mathbf{r}_j, z_j) = -\frac{i}{\lambda z}\exp\left(\frac{2\pi i z_{ij}}{\lambda}\right)\exp\left(\frac{i\pi \mathbf{r}_j^2}{\lambda z_{ij}}\right)\Im[\psi_\lambda(\mathbf{r}_i, z_i)] \quad (3)$$

The intensity distribution at z_j for polychromatic diffraction is given by the modulus squared of $\psi_\lambda(\mathbf{r}_j, z_j)$ for each value of λ weighted by the fractional contribution ξ_λ to the entire spectrum at that wavelength:

$$I(\mathbf{r}_j, z_j) = \int \xi_\lambda \left|\psi_\lambda(\mathbf{r}_j, z_j)\right|^2 \mathrm{d}\lambda \quad (4)$$

Defining $\Delta\lambda$ to be the separation between neighbouring sampling points of the spectrum, we find that a physical scaling of the intensity distribution at one value of λ is sufficient to obtain the distribution at an adjacent wavelength if $\Delta\lambda$ is sufficiently small. For example, if the largest wavelength sampled, λ_{max}, is used to propagate the sample ESW according to equation (3), then changing between the intensity distribution for λ_{max} and that of the next smallest wavelength is achieved by rescaling $\mathbf{r}_j$ according to $\mathbf{r}_j(\lambda_{max} - \Delta\lambda)/\lambda_{max}$.

Algorithm. The image reconstruction for polyCDI is be performed using the following algorithm:

(1) An initial guess is made for the sample ESW: $\psi(\mathbf{r}_i, z_i)$.
(2) The result is propagated to the far-field via equation (3) to give the central wavelength distribution $\psi_c(\mathbf{r}_j, z_j)$ and scaled by a factor appropriate to λ_{max} to yield $\psi(\mathbf{r}_j, z_j)_{\lambda_{max}}$.
(3) The positions $\mathbf{r}_j$ for the other sampled wavelengths are rescaled according to $\mathbf{r}_j(\lambda_{max} - \Delta\lambda)/\lambda_{max}$.
(4) The diffraction patterns from each sampled wavelength are calculated via interpolation onto the new set of points defined by the rescaled values for $\mathbf{r}_j$.
(5) The intensity distribution from each pattern is multiplied by a weighting factor determined by the relative contribution of each wavelength to the frequency spectrum: $\xi_\lambda|\psi_\lambda(\mathbf{r}_j, z_j)|^2$.
(6) The sum of the distributions for each sampling point approximates the integral in equation (4), which gives the calculated polychromatic diffraction pattern: $I(\mathbf{r}_j, z_j) = \int \xi_\lambda|\psi_\lambda(\mathbf{r}_j, z_j)|^2\ \mathrm{d}\lambda$.
(7) The modulus constraint is imposed using $|\psi_c(\mathbf{r}_j, z_j)| * \sqrt{I(\mathbf{r}_j, z_j)_{meas}}/\sqrt{I(\mathbf{r}_j, z_j)}$ where $I(\mathbf{r}_j, z_j)_{meas}$ is the measured intensity from the experiment.
(8) With the amplitude updated, the phase of $\psi_c(\mathbf{r}_j, z_j)$ is retained and the ESW propagated back to the sample plane to give $\psi(\mathbf{r}_i, z_i)$, after which the support constraint is imposed.
(9) Steps 1 to 9 are repeated and the progress of the reconstruction monitored using an error metric defined as $\chi^2 = \left(\sqrt{I(\mathbf{r}_j, z_j)_{meas}} - \sqrt{I(\mathbf{r}_j, z_j)}\right)^2 / I(\mathbf{r}_j, z_j)$.

The standard 'recipe' adopted for the reconstructions was four cycles of 100 iterations of ER followed by 50 of HiO, after which the polyCDI algorithm would generally converge and the remainder of the iterations (up to a maximum of 1,000) were carried out using ER with a fixed support. Using the method described in ref. 9, the effects of partial spatial coherence can be included in the polyCDI algorithm by a multimodal propagation of the central wavelength to the far-field. This requires full knowledge of the coherence characteristics of the source in order to specify the modal occupancies. Owing to the additional blurring caused by partial spatial coherence, however, the effective bandwidth that can be tolerated using polyCDI will

© 2011 Macmillan Publishers Limited. All rights reserved.

be reduced. The criteria for being able to retrieve the phase of the diffraction pattern are outlined in Supplementary Data S2.

Received 2 February 2011; accepted 16 May 2011;
published online 26 June 2011

References

1. Chapman, H. N. & Nugent, K. A. Coherent lensless X-ray imaging. *Nature Photon.* **4,** 833–839 (2010).
2. Emma, P. *et al.* First lasing and operation of an angstrom-wavelength free-electron laser. *Nature Photon.* **4,** 641–647 (2010).
3. Miao, J. *et al.* Extending the methodology of X-ray crystallography to allow imaging of micrometre-sized non-crystalline specimens. *Nature* **400,** 342–344 (1999).
4. Nugent, K. A. Coherent methods in the X-ray sciences. *Adv. Phys.* **59,** 1–99 (2010).
5. Larabell, C. A. & Le Gros, M. A. X-ray tomography generates 3-D reconstructions of the yeast, *Saccharomyces cerevisiae*, at 60-nm resolution. *Mol. Biol. Cell* **15,** 957–962 (2004).
6. Shen, Q., Bazarovc, I. & Thibault, P. Diffractive imaging of nonperiodic materials with future coherent X-ray sources. *J. Synchrotron Radiat.* **11,** 432–438 (2004).
7. Huang, X. J. *et al.* Signal-to-noise and radiation exposure considerations in conventional and diffraction X-ray microscopy. *Opt. Express* **17,** 13541–13553 (2009).
8. Wang, Y., Yun, W. & Jacobsen, C. Achromatic Fresnel optics for wideband extreme-ultraviolet and X-ray imaging. *Nature* **424,** 50–53 (2003).
9. Chapman, H. N. *et al.* High-resolution ab initio three-dimensional X-ray diffraction microscopy. *J. Opt. Soc. Am. A 2006.* **23,** 1179–1200 (2006).
10. Whitehead, L. W. *et al.* Diffractive imaging using partially coherent X Rays. *Phys. Rev. Lett.* **103,** 243902 (2009).
11. Chen, M-C. *et al.* Bright, coherent, ultrafast soft X-ray harmonics spanning the water window from a tabletop light source. *Phys. Rev. Lett.* **105,** 173901 (2010).
12. Quiney, H. M. Coherent diffractive imaging using short wavelength light sources. *J. Mod. Opt.* **57,** 1–57 (2010).
13. Chen, B. *et al.* Multiplewavelength diffractive imaging. *Phys. Rev. A* 2009. **79,** 023809 (2009).
14. McNulty, I. *et al.* A beamline for 1–4 keV microscopy and coherence experiments at the Advanced Photon Source. *Rev. Sci. Instrum.* **67,** 3372 (1996).
15. Paterson, D. *et al.* Spatial coherence measurement of X-ray undulator radiation. *Opt. Commun.* **195,** 79–84 (2001).
16. Tanaka, T. & Kiamura, H. SPECTRA—a synchrotron radiation calculation code. *J. Synchrotron Radiat.* **8,** 1221–1228 (2001).
17. Kim, K-J. Characteristics of synchrotron radiation, in *X-Ray Data Booklet* Section 2.1 (Lawrence Berkeley National Laboratory (LBNL), 2009).
18. Walton, A. J. The Abbe theory of imaging: an alternative derivation of the resolution limit. *Eur. J. Phys.* **7,** 62–63 (1986).
19. Williams, G. J. *et al.* Coherent diffractive imaging and partial coherence. *Phys. Rev. B* **75,** 104102 (2007).
20. Fienup, J. R. Reconstruction of a complex-valued object from the modulus of its Fourier transform using a support constraint. *J. Opt. Soc. Am. A* **4,** 118–123 (1987).

Acknowledgements

The authors acknowledge the support of the Australian Research Council Centre of Excellence for Coherent x-ray Science and the Australian Synchrotron Research Program. Use of the Advanced Photon Source was supported by the US Department of Energy, Office of Science, Office of Basic Energy Sciences (contract no. DE-AC02-06CH11357).

Author contributions

B.A carried out the experimental data analysis. L.W.W. and H.M.Q. carried out the simulation studies. L.W.W., A.G.P., G.J.W., C.T.P., G.C., C.A.H., D.J.V., K.A.N and I.McN. were responsible for carrying out the experiment. E.B. prepared and characterized the samples. A.G.P. was responsible for project planning, and L.W. and H.M.Q. were responsible for developing the polychromatic diffraction algorithm. H.M.Q. determined the maximum allowed bandwidth for the algorithm (Supplementary Information 2). All authors contributed to the writing of the manuscript. Credit for the initial idea and concept go to K.A.N and I.McN.

Additional information

The authors declare no competing financial interests. Supplementary information accompanies this paper at www.nature.com/naturephotonics. Reprints and permission information is available online at http://www.nature.com/reprints/. Correspondence and requests for materials should be addressed to K.A.N.

© 2011 Macmillan Publishers Limited. All rights reserved.